Supplemental Materials

Molecular Biology of the Cell

Goss et al.

SUPPLEMENTAL MATERIALS

Characterization of the roles of Blt1p in fission yeast cytokinesis

John W. Goss, Sunhee Kim, Hannah Bledsoe, and Thomas D. Pollard

SUPPLEMENTAL RESULTS

Blt1p is not required for contractile ring assembly

We used time-lapse imaging of live cells expressing cytokinesis node proteins fluorescently tagged at their native promoters to evaluate whether Blt1p regulates their localization, thereby contributing to the onset of contractile ring constriction.

F-BAR domain-containing protein Cdc15p contributes to anchoring the contractile ring to the cell wall. Consistent with previous reports, Cdc15p localized to cytokinesis nodes at the equator at time -3 ± 2 minutes, and these nodes coalesced into the fully formed contractile ring at time +23 ± 2 min in wild type cells (Supplemental Figure S1, A-B) (Wu et al, 2006; Laporte et al, 2011). Additionally, the concentration of Cdc15p molecules at the cleavage furrow increased after SPB separation and peaked as the ring matured in preparation for constriction (Wu and Pollard, 2005; Supplemental Figure S1C). We observed no change in the spatial or temporal localization of Cdc15p to either cytokinesis nodes (-3 ± 3 min) or the contractile ring (24 ± 3 min) in *blt1*Δ cells (Supplemental Figure S1A-B), and the total number of Cdc15p molecules present in the cleavage furrow was also unchanged upon $blt1^{+}$ deletion (Supplemental Figure S1C).

Conventional myosin II consisting of heavy chain Myo2p, regulatory light chain Rlc1p and essential light chain Cdc4p contributes to condensation of cytokinesis nodes and constriction of the contractile ring. In wild type cells, Myo2p and Rlc1p localized to cytokinesis nodes at -9 ± 3 and -9 ± 2 minutes, respectively, and condensed into the fully formed CRs at +22 ± 2 and +23 ± 3 min (Supplemental Figure S1, D-E, Supplemental Figure S2A) (Wu et al, 2006; Laporte et al, 2011). Likewise, the number of Myo2p and Rlc1 at the cleavage furrow increased after SPB separation and peaked at ~5,000 after maturation of the contractile ring and onset of constriction (Supplemental Figure S1F, Supplemental Figure S2B) (Wu and Pollard, 2005). The absence of Blt1p did not affect the timing of Myo2p and Rlc1p localization to cytokinesis nodes (-9 ± 4 and

-9 ± 4 min, respectively) and the contractile ring (+23 ± 2 and +22 ± 3 min) (Supplemental Figure S1F, Supplemental Figure S2B), and there was no statistically significant difference in the total number of Myo2p and Rlc1p molecules present in the cleavage furrow upon *blt1*$^{+}$ deletion (Supplemental Figure S1F, Supplemental Figure S2B).

Unconventional myosin II, Myp2p is recruited to cytokinesis nodes as they condense into the contractile ring and contributes to ring constriction. Consistent with previous findings Myp2p localized to cytokinesis nodes at +15 ± 3 minutes in wild type cells (Supplemental Figure S2, C-D) (Wu et al, 2006), and the number of Myp2p molecules present in the cleavage furrow peak at ~2,000 after maturation of the contractile ring and onset of constriction (Supplemental Figure S2E) (Wu and Pollard, 2005). Myp2p localized to cytokinesis nodes at a similar time (+15±2 minutes) (Supplemental Figure S2, C-D) and was present at the cleavage furrow at the same amount in *blt1*Δ cells (Supplemental Figure S2E).

Cytokinesis protein Blt1p

SUPPLMENTAL TABLE 1: Strain list

Strain	**Genotype**	**Source**
IH2939	*h- mob1-R4, ura4-D18*	Lab stock
IRT13	*h- rng2-D5, ade6-M210, leu1-32, ura4-D18*	Lab stock
JG1-1	*h- blt1Δ::natMX6, ade6-M210, leu1-32, ura4-D18*	This study
JG3-4	*h- blt1-mEGFP-kanMX6, sad1-RFP-kanMX6, ade6-M21X, leu1-32, ura4-D18*	This study
JG12	*blt1Δ::natMX6, cdc15-mEGFP-kanMX6, sad1-RFP-kanMX6, ade6-M210, leu1-32, ura4-D18*	This study
JG13	*blt1Δ::natMX6, kanMX6-*$P_{myo2}{}^{+}$*-mEGFP-myo2, sad1-RFP-kanMX6, ade6-M210, leu1-32, ura-D18*	This study
JG16	*blt1Δ::natMX6, myo2-E1, ade6-M216, leu1-32, ura4-D18*	This study
JG17	*blt1Δ::natMX6, rng2-D5, ade6-M210, leu1-32, ura4-D18*	This study
JG19	*blt1Δ::natMX6, cdc15-127, ade6-M216, leu1-32, ura4-D18, his7-366*	This study
JG20	*blt1Δ::natMX6, cdc11-19, ade6-M216, leu1-32, ura4-D18, his7-366*	This study
JG21	*blt1Δ::natMX6, cdc7-24, ade6-M216, leu1-32, ura4-D18, his7-366*	This study
JG22	*blt1Δ::natMX6, cdc25-22, ade6-M216, leu1-32, ura4-D18*	This study
JG25	*blt1Δ::natMX6, sid4-A1, ade6-M216, leu1-32, ura4-D18*	This study
JG26	*blt1Δ::natMX6, sid1-125, ade6-M216, leu1-32, ura4-D18*	This study
JG29	*blt1Δ::natMX6, cdc14-118, ade6-M216, leu1-32, ura4-D18*	This study
JG31-1	*blt1Δ::natMX6, sid2-250, ade6-M210, leu1-32, ura4-D18*	This study
JG38	*blt1Δ::natMX6, cdc16-116, ade6-M216, leu1-32, his7-366*	This study
JG39	*blt1Δ::natMX6, cdc3-6, ade6-M216, leu1-32, ura4-D18, his7-366*	This study
JG40	*blt1Δ::natMX6, cdc4-8, ade6-M216, leu1-32, ura4-D18, his7-366*	This study
JG41	*blt1Δ::natMX6, cdc8-27, ade6-M216, leu1-32, ura4-D18, his7-366*	This study
JG43	*blt1Δ::natMX6, spg1-106, ade6-M216, leu1-32, ura4-D18*	This study
JG45	*blt1Δ::natMX6, cdc2-M26, ade6-M216, leu1-32, ura4-D18, his7-366*	This study
JG49-2	*h+ blt1Δ::natMX6, sid2-mEGFP-kan, ade6-M210, leu1-32, ura4-D18*	This study
JG50-12	*h- blt1Δ::natMX6, mob1-mEGFP-kan ade6-M210, leu1-32, ura4-D18*	This study
JG68-3	*h- blt1Δ::natMX6, mob1-R4, ade6-M210, leu1-32, ura4-D18*	This study
JG72-1	*blt1Δ::natMX6, plo1-24C, ade6-M210, leu1-32, ura4-D18*	This study
JG79-4A	*h+ blt1Δ::natMX6, kanMX6-*$P_{bgs1}{}^{+}$*-mEGFP-bgs1 sad1-RFP-kanMX6 ade6-M210, leu1-32, ura4-D18*	This study
JG93-1	*blt1Δ::natMX6, mid1Δ::kanMX6, ade6-M216, leu1-32, ura4-D18, his3-D1*	This study

Cytokinesis protein Blt1p

JG114	*gef2Δ::kanMX6, mob1-mEGFP-kanMX6, ade6-M210, leu1-32, ura4-D18*	This study
JG115-4D	*gef2Δ::kanMX6, sid2-mEGFP-kan, ade6-M210, leu1-32, ura4-D18*	This study
JG123-2B	*blt1Δ::natMX6, rlc1-YFP-kanMX6, sad1-CFP-kanMX6, ade6-M210, leu1-32, ura4-D18*	This study
JG125	*kanMX6-3nmt-mob1-mYFP, rlc1-CFP-kan, ade6-m210, leu1-32, ura4-D18*	This study
JG128	*kanMX6-3nmt-sid2-mYFP, rlc1-CFP-kan, ade6-m210, leu1-32, ura4-D18*	This study
CB96	*arp2-mEGFP-kanMX6, ade6-M210, leu1-32, ura4-D18*	Lab stock
CB97	*arp3-mEGFP-kanMX6, ade6-M210, leu1-32, ura4-D18*	Lab stock
CB106	*arp2-mYFP-kanMX6, ade6-M210, leu1-32, ura4-D18*	Lab stock
CB107	*arp3-mYFP-kanMX6, ade6-M210, leu1-32, ura4-D18*	Lab stock
CM26-3	*h- sid2-mEGFP-kan, ade6-M210, leu1-32, ura4-D18*	Lab stock
CM32-4	*h+ mob1-mEGFP-kan, ade6-M210, leu1-32, ura4-D18*	Lab stock
CM85	*h- mob1-R4, ade6-M210, leu1-32, ura4-D18*	Lab stock
EMM1-4	*h+ cdr2-mEGFP-kanMX6, sad1-RFP-kanMX6, ade6-M21X, leu1-32, ura4-D18*	This study
IRT161	*h+ kanMX6-*P_{bgs1}^{+}*-mEGFP-bgs1 sad1-RFP-kanMX6 ade6-M210, leu1-32, ura4-D18*	Lab stock
JQ1109	*kanMX6-*P_{myo2}^{+}*-mEGFP-myo2, ade6-M210, leu1-32, ura4-D18*	Lab stock
JQ1110	*kanMX6-*P_{myo2}^{+}*-mYFP-myo2, ade6-M210, leu1-32, ura4-D18*	Lab stock
JQ1114	*ain1-mEGFP-kanMX6, ade6-M210, leu1-32, ura4-D18*	Lab stock
JQ1145	*ain1-mYFP-kanMX6, ade6-M210, leu1-32, ura4-D18*	Lab stock
JW81	*h- ade6-M210, leu1-32, ura4-D18*	Lab stock
JW820	*h+ mid1-YFP-kanMX6, sad1-CFP-kanMX6, ade6-M210, leu1-32, ura4-D18*	Lab stock
JW834	*h- kanMX6-*P_{myo2}^{+}*-YFP-myo2, sad1-CFP-kanMX6, ade6-M210, leu1-32, ura-D18*	Lab stock
JW979	*h- cdc15-YFP-kanMX6, sad1-CFP-kanMX6, ade6-M210, leu1-32, ura4-D18*	Lab stock
JW991	*rlc1-YFP-kanMX6, sad1-CFP-kanMX6, ade6-M210, leu1-32, ura4-D18*	Lab stock
JW1009	*h+ cdc25-22, ade6-M210, leu1-32, ura4-D18*	Lab stock
JW1033	*h- sid4-A1, ade6-M210, leu1-32, ura4-D18*	Lab stock
JW1034	*h+ sid2-250, ade6-M21X, leu1-32, ura4-D18*	Lab stock
JW1036	*h+ sid1-125, ade6-M21X, leu1-32, ura4-D18*	Lab stock
JW1826	*h+ gef2Δ::kanMX6 ade6-M210, leu1-32, ura4-D18*	JQ Wu
JW4227	*kanMX6-*P_{gef2}^{+}*-mEGFP-4Gly-gef2, sad1-tdTomato-natMX6, ade6-*	JQ Wu

Cytokinesis protein Blt1p

	M210, leu1-32, ura4-D18	
JW4237	*Blt1Δ::kanMX6, kanMX6-*P_{gef2}^{+}*-mEGFP-4Gly-gef2, sad1-tdTomato-natMX6, ade6-M210, leu1-32, ura4-D18*	JQ Wu
MB7	*h- cdc4-8, ade6-M216, leu1-32, ura4-D18, his7-366*	Lab stock
MB8	*h- cdc3-6, ade6-M216, leu1-32, ura4-D18, his7-366*	Lab stock
MB9	*h- cdc8-27, ade6-M216, leu1-32, ura4-D18, his7-366*	Lab stock
MB29	*h+ cdc14-118, ade6-M216, leu1-32, his7-366*	Lab stock
MB30	*h+ cdc15-127, ade6-M216, leu1-32, ura4-D18, his7-366*	Lab stock
MB32	*h+ cdc16-116, ade6-M216, leu1-32, his7-366*	Lab stock
MB34	*h- cdc7-24, ade6-M216, leu1-32, ura4-D18, his7-366*	Lab stock
MB36	*h- cdc11-19, ade6-M216, leu1-32, ura4-D18, his7-366*	Lab stock
MB59	*h- myo2-E1, ade6-M216, leu1-32, ura4-D18*	Lab stock
MB61	*h- cdc2-M26, ade6-M216, leu1-32, ura4-D18, his7-366*	Lab stock
SSP2-3	*mid1Δ::kan, ade6-M210, leu1-32, ura4-D18, his3-D1*	Lab stock
TP226	*arpc5-mEGFP-kanMX6, ade6-M210, leu1-32, ura4-D18*	Lab stock
TP227	*arpc5-mYFP-kanMX6, ade6-M210, leu1-32, ura4-D18*	Lab stock
TP237	*acp2-mEGFP-kanMX6, ade6-M210, leu1-32, ura4-D18*	Lab stock
TP340	*acp2-mYFP-kanMX6, ade6-M210, leu1-32, ura4-D18*	Lab stock
TP345	*fim1-mYFP-kanMX6, ade6-M210, leu1-32, ura4-D18*	Lab stock
TP347	*aim1-mEGFP-kanMX6, ade6-M210, leu1-32, ura4-D18*	Lab stock
YDM114	*h+ plo1-24C, ade6-M120, leu1-32, ura4-D18*	Lab stock
YDM430	*h+ spg1-106, ade6-M210, leu1-32, ura4-D18*	Lab stock

SUPPLEMENTAL FIGURE S1. Mutant *blt1*Δ cells recruit Cdc15p and Myo2p normally to nodes and the contractile ring. Times are in min with spindle pole body separation at time zero. Open symbols are wild type cells and filled symbols are *blt1*Δ cells. (A) Time series of fluorescence micrographs at 4 min intervals of (top row) wild type *blt1*$^{+}$ cells expressing Cdc15p-mEGFP (green) and Sad1p-RFP (red) and (bottom row) *blt1*Δ cells expressing Cdc15p-mYFP (green) and Sad1p-CFP (red). (B) Time courses of the accumulation of cells ±1 SD with (O, ●) Cdc15p in cortical nodes and (□, ■) nodes condensed into a contractile ring in 41 wild type cells and 43 *blt1*Δ cells. None of these mean values differed significantly between the strains. (C) Time course of the mean number ±1 SD of Cdc15p molecules localized at the cleavage site in wild type (black line; n = 23) and *blt1*Δ (grey line; n =21) cells. None of these mean values differed significantly between the strains. (D) Time series of fluorescence micrographs at 4 min intervals of (top row) wild type *blt1*$^{+}$ cells expressing Myo2p-mEGFP (green) and Sad1p-RFP (red) and (bottom row) *blt1*Δ cells expressing Myo2p-mYFP (green) and Sad1p-CFP (red). (E) Time courses of the accumulation of cells ±1 SD with (O, ●) Myo2p in cortical nodes and (□, ■) nodes condensed into a contractile ring in 24 wild type cells and 23 *blt1*Δ cells. None of these mean values differed significantly between the strains. (F) Time course of the mean number ±1 SD of Myo2p molecules localized at the cleavage furrow in 24 wild type cells (black line) and 23 *blt1*Δ cells (grey line). None of these mean values differed significantly between the strains. Scale bar = 5 μm.

SUPPLEMENTAL FIGURE S2. Mutant *blt1*Δ cells recruit Rlc1p and Myp2 normally to nodes and the contractile ring. Times are in min with spindle pole body separation at time zero. Open symbols are wild type cells and filled symbols are *blt1*Δ cells. (A) Time courses of the accumulation of cells ±1 SD with (O, ●) Rlc1p in cortical nodes and (□, ■) nodes condensed into a contractile ring in 33 wild type cells and 43 *blt1*Δ cells expressing Rlc1p-mEGFP and Sad1-mRFP. None of these mean values differed significantly between the strains. (B) Time course of the mean number ±1 SD of Rlc1p molecules localizing to the cleavage site in 23 wild type cells (black line) and 21 *blt1*Δ cells (grey line). None of these mean values differed significantly between the strains. (C) Time series of fluorescence micrographs at 4 min intervals of (top row) wild type *blt1*$^{+}$cells and (bottom row) *blt1*Δ cells expressing Myp2p-mYFP (green) and Sad1p-CFP (red). (D) Time courses of the accumulation of cells ±1 SD with (O, ●) Myp2p in cortical nodes in 27 wild type cells and 22 *blt1*Δ cells. None of these mean values differed significantly between the strains. (E) Time course of the mean number ±1 SD of Myp2p molecules localized at the cleavage site in 27 wild type cells (black line) and 22 *blt1*Δ cells (grey line). None of these mean values differed significantly between the strains. Scale bar = 5 μm.

SUPPLEMENTAL FIGURE S3. Blt1Δ cells progress through the stages of mitosis at a normal rate. Times are in min with spindle pole body (SPB) separation at time zero. (A) Time series of fluorescence micrographs at 4 min intervals of wild type (*blt1*$^{+}$, top row) or *blt1*Δ (bottom row) cells expressing Sad1-RFP. Scale bar = 0.5 μm. (B) Time courses of the accumulation of 30 wild type cells (open symbols) and 30 *blt1*Δ cells (filled symbols) at mitotic landmarks ±1 SD: (O, ●) completion of SPB localization to opposite sides of the nucleus (anaphase A); (□, ■) completion of SPB movement to the poles of the cells (anaphase B); and (Δ, ▲) onset of SPB movement back to the cell equator (telophase). None of these mean values differed significantly between the strains.

Cytokinesis protein Blt1p

SUPPLEMENTAL FIGURE S4. SIN pathway components *sid2-250* and *mob1-R4* mutants have a synthetic genetic interaction with *blt1*Δ. Wild type, single- and double-mutant cells were grown in exponential phase and 10^4 cells were plated, spread and grown at (A) 25°C, (B) 30°C, or (C) 36°C for 48 h (B-C) or 72 h (A).

SUPPLEMENTAL FIGURE S5. Counts of total protein molecules. (A-D) 20 wild type cells (black line) and 20 *blt1*Δ cells (grey line) have the same total numbers of Mob1p, Sid2p, Clp1p, and Bgs1p molecules. Times are in min with spindle pole body separation at time zero. Time course of the mean number ± 1 SD of total molecules of (A) Mob1p-mYFP, (B) Sid2p-mYFP, (C) Clp1p-mEGFP and (D) Bgs1p mEGFP. (E, F) Time course of mean number ± 1 SD of (E) nmt-Mob1p-mYFP molecules and (F) nmt-Sid2p-mYFP molecules in 0 µM thiamine (black line) and 15 µM thiamine (grey line). *P-value* <0.0001 for all time points in (E) and (F).

SUPPLEMENTAL FIGURE S6. Accumulation of Mob1p and Sid2p contributes to contractile ring constriction. Times are in min with spindle pole body separation at time zero. (A-C) *3nmt-mob1p-mYFP* cells expressing Rlc1p-CFP (red). (A) Time series of fluorescence micrographs at 4 min intervals of cells grown for 10 h in (top row) 0 µM thiamine or (bottom row) 15 µM thiamine (15 cells each condition) to partially deplete protein expression. Scale bar = 5 µm. (B) Time courses of the accumulation of cells ±1 SD with constricting contractile rings in (O) 0 µM thiamine or (●) 15 µM thiamine (15 cells each condition). Asterisks indicate time points where the mean values of the two cell types differed with *p-values* <0.0001. (C) Time course of the mean number ±1 SD of 3nmt-Mob1p-mYFP molecules localized at the cleavage site without thiamine (black line) or 15 µM thiamine (grey line). Asterisks indicate time points where the mean values of the two cell types differed with *p-values* <0.001. (D-F) *3nmt-sid2p-mYFP* cells expressing Rlc1p-CFP (red). (D) Time series of fluorescence micrographs at 4 min intervals of cells grown for 10 h in (top row) 0 µM thiamine or (bottom row) 15 µM thiamine (15 cells each condition) to partially deplete protein expression. Scale bar = 5 µm. (E) Time courses of the accumulation of cells ±1 SD with constricting contractile rings constriction (O) without thiamine or (●) 15 µM thiamine. Asterisks indicate time points where the mean values of the two cell types differed with *p-values* <0.0001. (F) Time course of the mean number ±1 SD of 3nmt-Sid2p-mYFP molecules localized at the cleavage site without thiamine (black line) or 15 µM thiamine (grey line). Asterisks indicate time points where the mean values of the two cell types differed with *p-values* <0.001.

SUPPLEMENTAL FIGURE S7. Lack of effects of repression of Mod1p or Sid2p expression on their total numbers at SPBs or progression of cells through mitosis. Times are in min with spindle pole body (SPB) separation at time zero. (A, C) Time courses of the mean number ±1 SD of (A) *3nmt*-Mob1p-mYFP or (C) *3nmt*-Sid2p-mYFP at both SPB without thiamine (black line; 25 cells) or 15 µM thiamine to repress expression (grey line; 24 cells). None of these mean values differed significantly between the strains. (B, D) Time courses of the accumulation of (B) *3nmt*-Mob1-mYFP cells and (D) *3nmt*-Sid2p-mYFP cells at mitotic landmarks ±1 SD with (open symbols) 0 µM thiamine or (filled symbols) 15 µM thiamine: (O, ●) completion of SPB localization to opposite sides of the nucleus (anaphase A); (□, ■) completion of SPB movement to the poles of the cells (anaphase B); and (Δ, ▲) onset of SPB movement back to the cell equator (telophase). Numbers of cells scored: 25 3nmt-Mob1-YFP cells without thiamine; 24 3nmt-Mob1-YFP cells with 15 µM thiamine; 25 3nmt-Sid2-YFP cells without thiamine; and 24 3nmt-Sid2-YFP cells with 15 µM thiamine. None of these mean values differed significantly between the strains.

SUPPLEMENTAL FIGURE S8. The absence of Blt1p reduces Gef2p localization to nodes and contractile rings. Times are in min with spindle pole body separation at time zero. (A) Time series of fluorescence micrographs at 8 min intervals of (top row) wild type *blt1*$^{+}$ or (bottom row) *blt1*Δ cells expressing mEGFP-Gef2p (green) and Sad1p-RFP (red). Scale bar = 5 µm. (B) Time courses of the accumulation of cells ±1 SD with Gef2p localized at the cleavage site in (O) 52 wild type cells and (●) 36 *blt1*Δ cells. Asterisks indicate time points where the mean values of the two cell types differed with *p-values* <0.0001. (C) Time course of the mean number ±1 SD of mEGFP-Gef2p molecules localized at the cleavage site in 29 wild type cells (black line) and 24 *blt1*Δ cells (grey line). Asterisks indicate time points where the mean values of the two cell types differed with *p-values* <0.001.

SUPPLEMENTAL FIGURE S9. Mutant *gef2*Δ cells recruit Mob1p normally to the division site. Times are in min with spindle pole body separation at time zero. (A) Time series of fluorescence micrographs at 4 min intervals of (top row) wild type *gef2*$^{+}$cells or *gef2*Δ cells expressing Mob1p-mEGFP (white). Scale bar = 5 μm. (B) Time courses of the accumulation of cells ±1 SD with Mob1p-mEGFP at the division plane in (O) 37 wild type cells and (●) 21 *gef2*Δ cells. None of these mean values differed significantly between the strains. (C) Time course of the mean number ±1 SD of Mob1p-mEGFP molecules localized at the cleavage furrow in 37 wild type cells (black line) and 21 *gef2*Δ cells (grey line). None of these mean values differed significantly between the strains.

Cytokinesis protein Blt1p

SUPPLEMENTAL FIGURE S10. Mutant *gef2*Δ cells recruit Sid2p normally to the division site. Times are in min with spindle pole body separation at time zero. (A) Time series of fluorescence micrographs at 4 min intervals of (top row) wild type *gef2*$^{+}$ cell and (bottom row) *gef2*Δ cells expressing Sid2p-mEGFP (white). Scale bar = 5 μm. (B) Time courses of the accumulation of cells ±1 SD with Sid2p at the division plane in (O) 24 wild type cells and (●) 22 *gef2*Δ cells. None of these mean values differed significantly between the strains. (C) Time course of the mean number ±1 SD of Sid2p molecules localized at the division site in 24 wild type cells (black line) and 19 *gef2*Δ cells (grey line). None of these mean values differed significantly between the strains.

SUPPLEMENTAL FIGURE S11. Offset division planes in *blt1*Δ cells. (A) Time series of reversed contrast fluorescence micrographs at 5 min intervals of *blt1*Δ cells expressing Cdc15-mEGFP. Time in min is shown with spindle pole body separation defined as time zero. (B) Histogram of the mean percentage ±1 SD of cells with a contractile ring that moved from its original position to become offset in 27 wild type *blt1*$^{+}$ cells and 29 *blt1*Δ cells. *P-value* <0.001. (C) Plot of the angle of the contractile ring relative to the plane perpendicular to the long axis of the cell (Θ°) ±1 SD vs. the longitudinal displacement of the contractile ring from the center of the cell (in μm) ±1 SD for (●) 27 wild type and (■) 29 *blt1*Δ cells. *P-value* <0.001 for both longitudinal displacement and angle of the contractile ring. Scale bar = 5 μm.

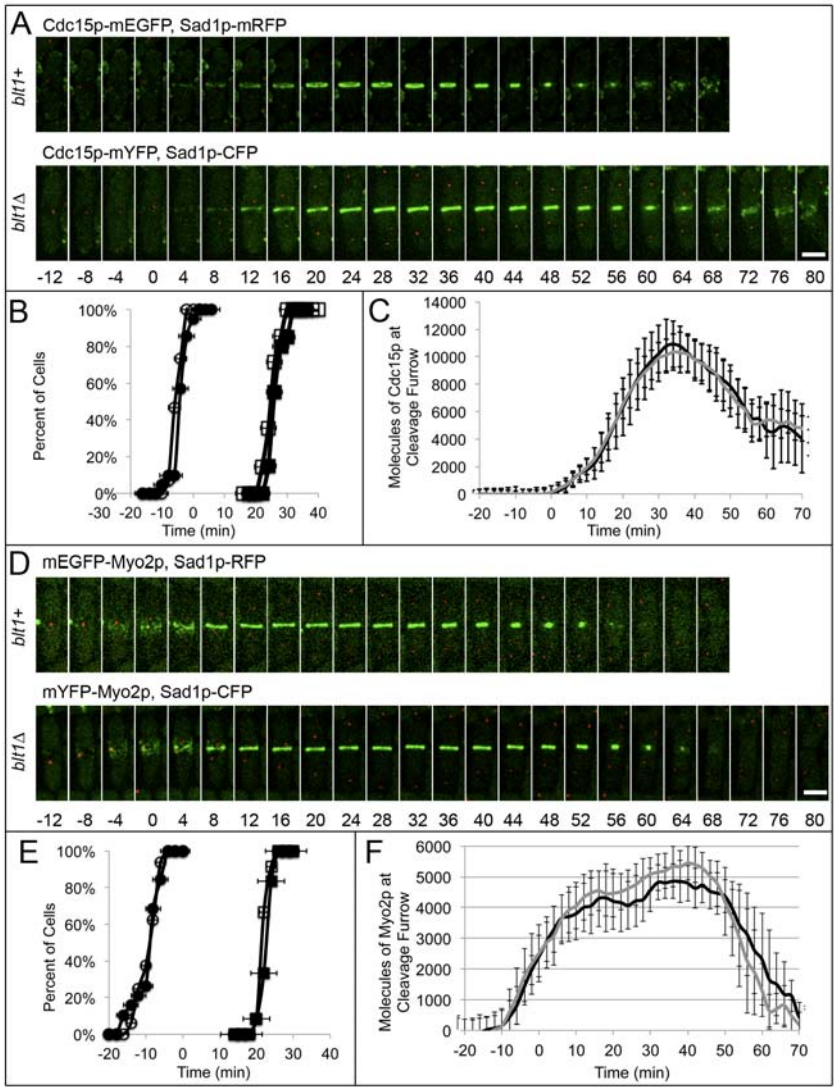

Supplmental Figure S1 - Goss et al

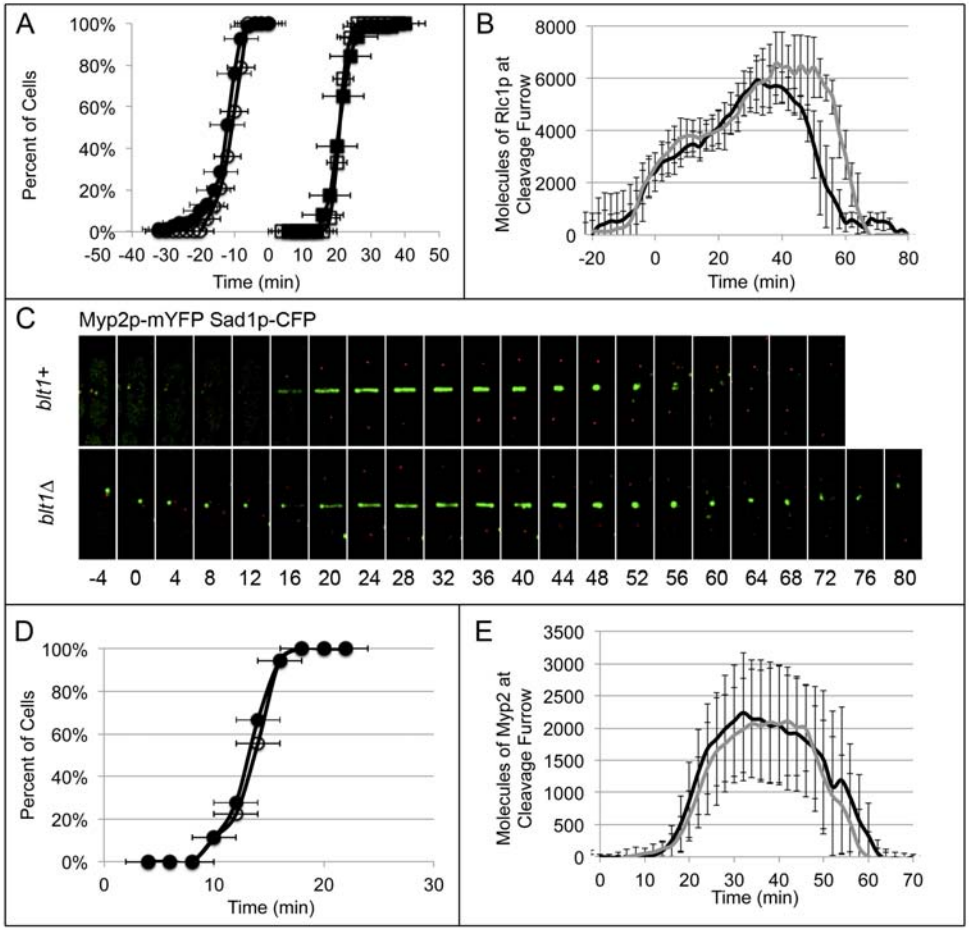

Supplemental Figure S2 - Goss et al

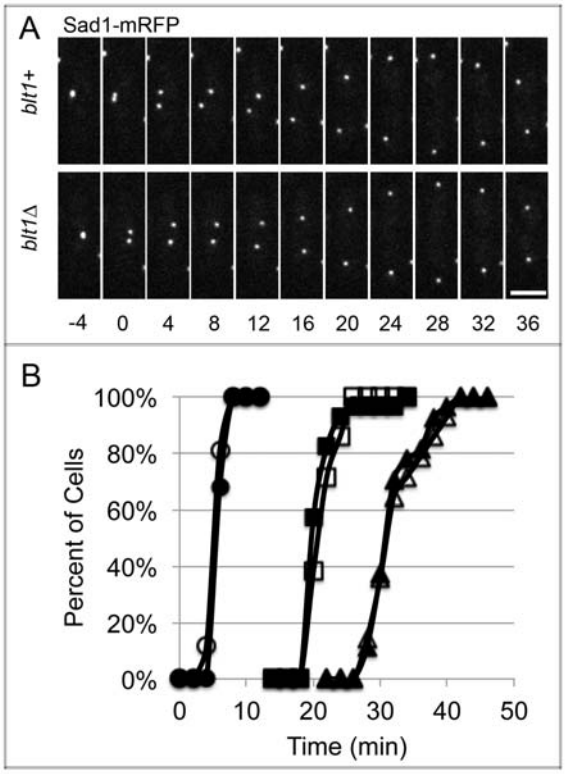

Supplemental Figure S3 - Goss et al

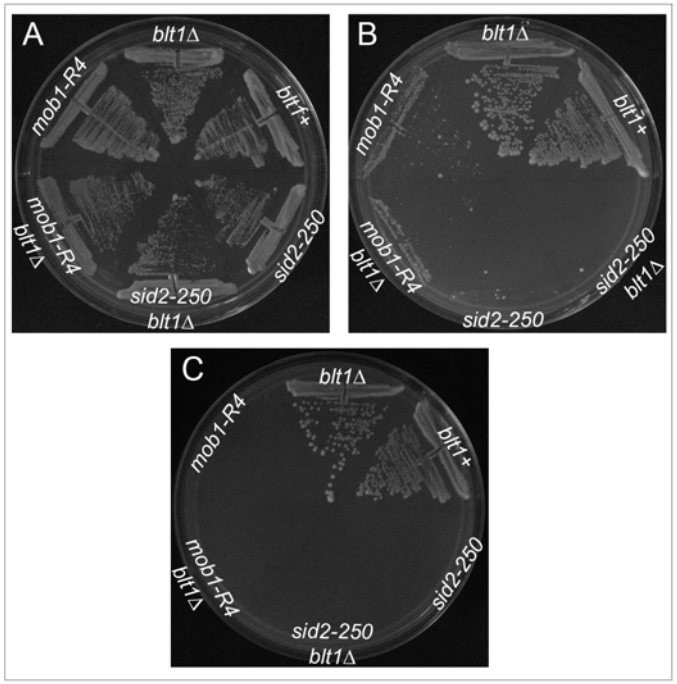

Supplemental Figure S4 - Goss et al

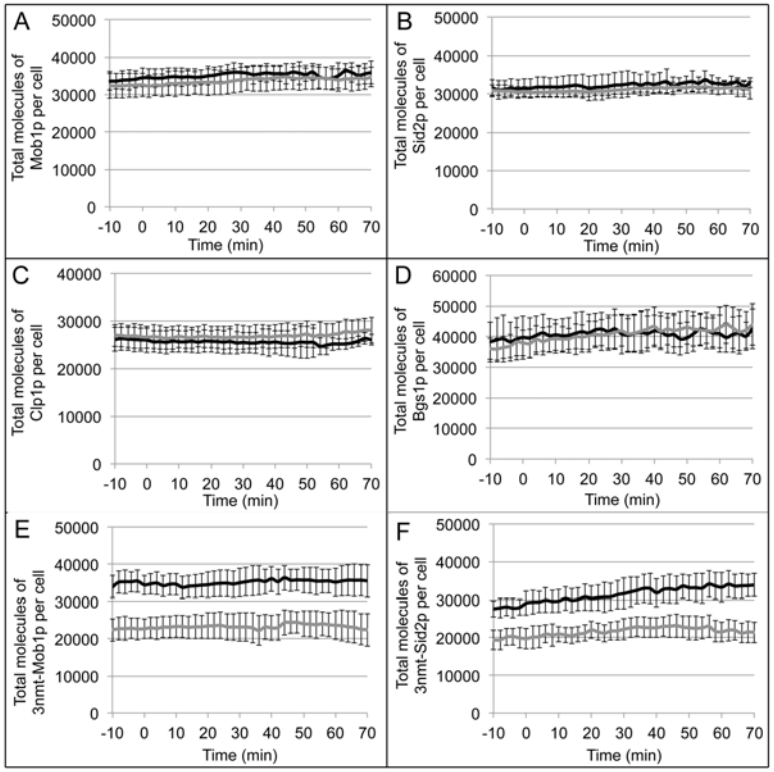

Supplemental Figure S5 - Goss et al

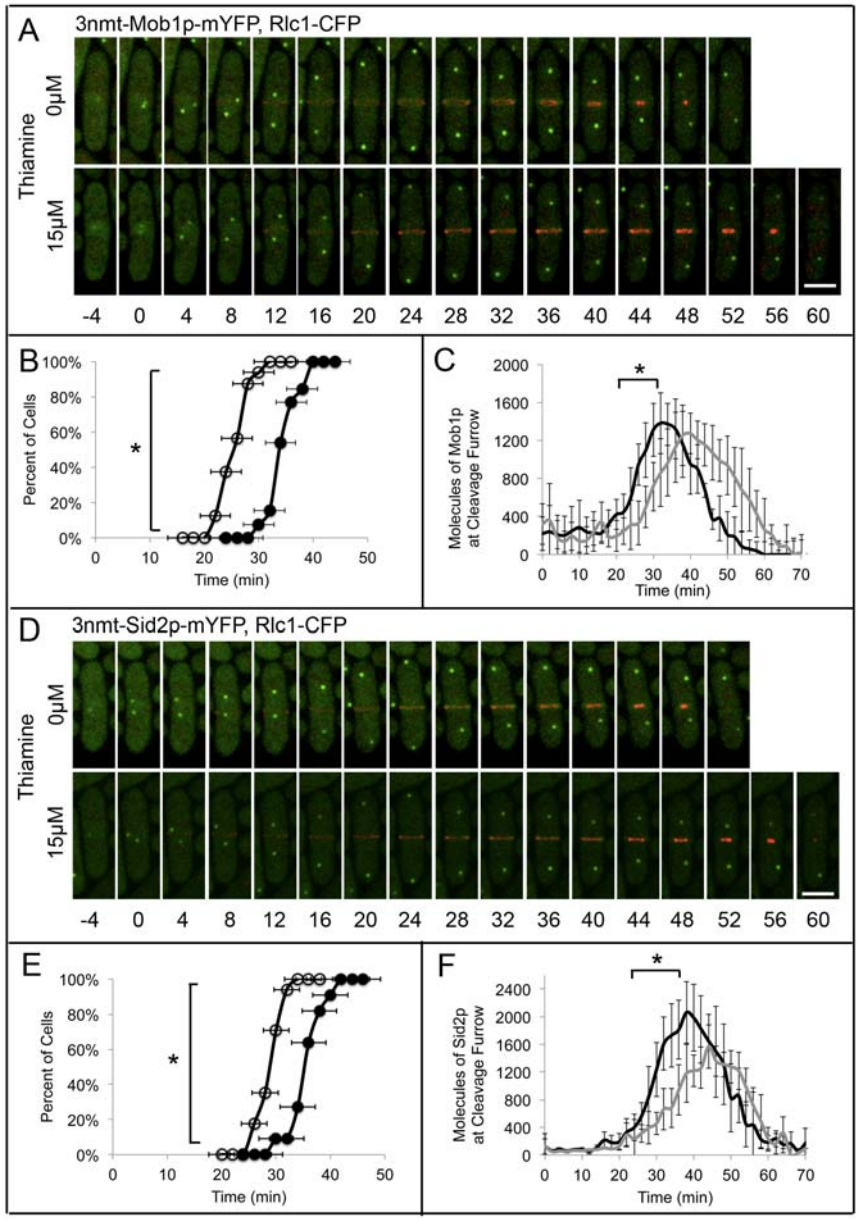

Supplemental Figure S6 - Goss et al

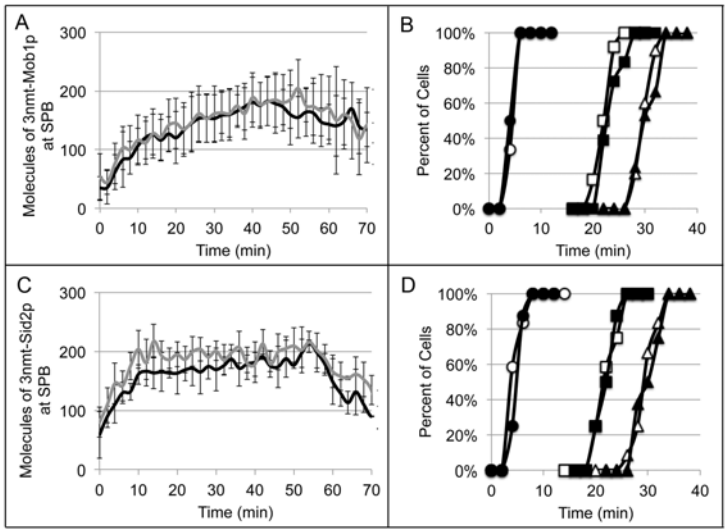

Supplemental Figure S7 - Goss et al

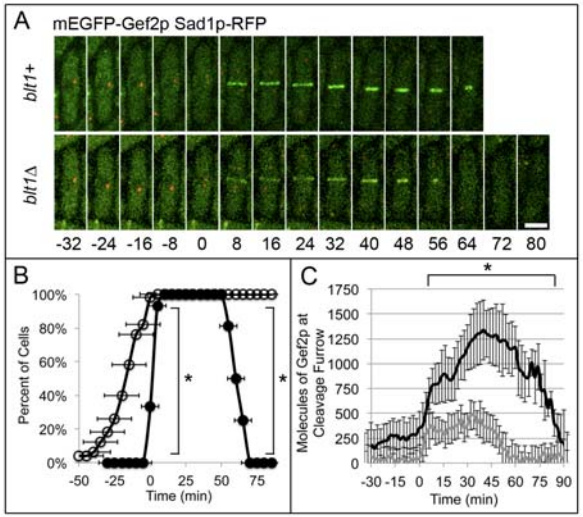

Supplemental Figure S8 - Goss et al

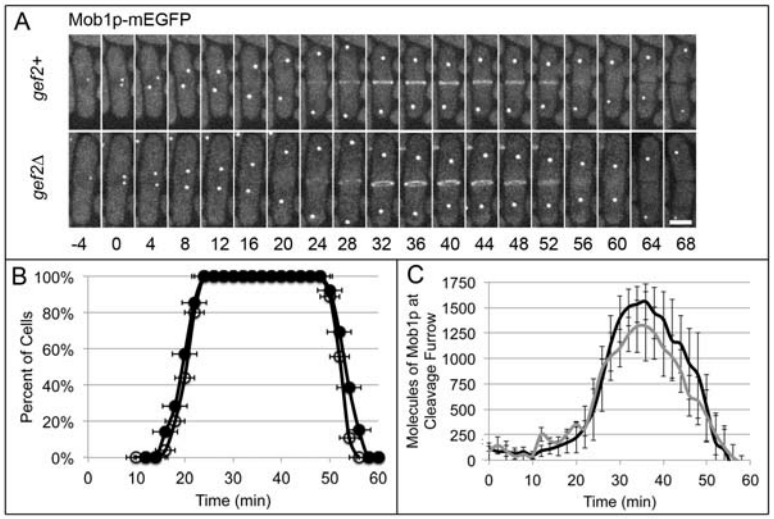

Supplemental Figure S9 - Goss et al

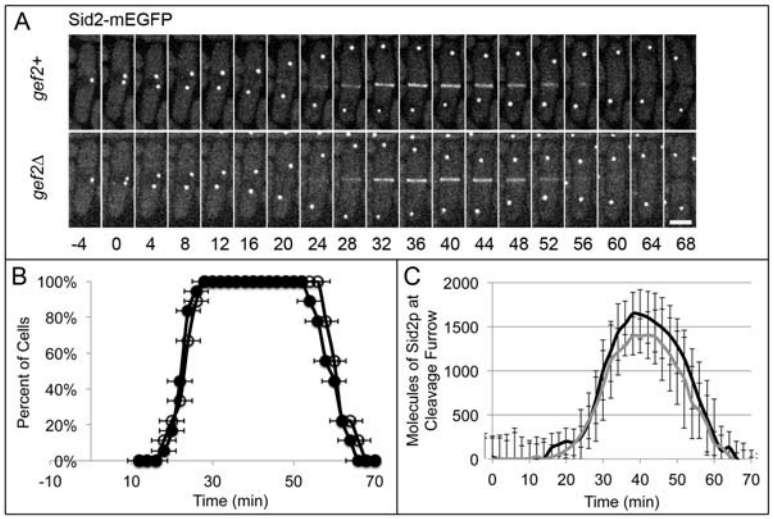

Supplemental Figure S10 - Goss et al

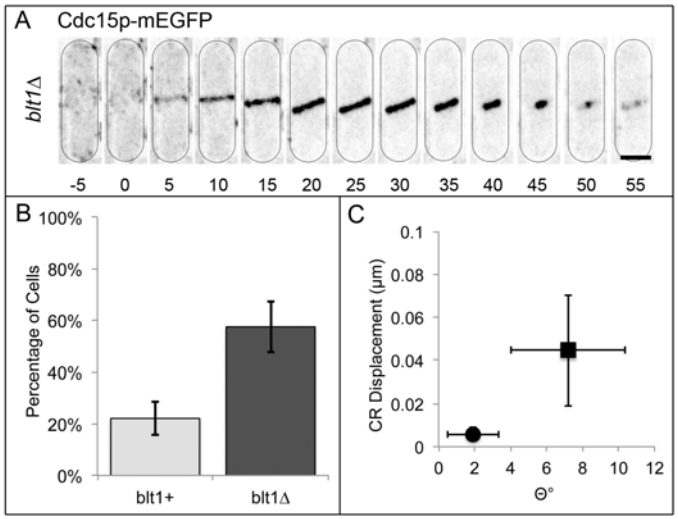

Supplemental Figure S11 - Goss et al